Doppler Reflectometry for the Investigation of poloidally propagating Density Perturbations

M Hirsch, E Holzhauer*, J Baldzuhn, B Kurzan

Max-Planck-Institut für Plasmaphysik, EURATOM Association, D-85748 Garching, Germany
*Institut für Plasmaforschung, Universität Stuttgart, D-70569 Stuttgart, Germany

A modification of microwave reflectometry is discussed where the direction of observation is tilted with respect to the normal onto the reflecting surface. The experiment is similar to scattering where a finite resolution in k-space exists but keeps the radial localization of reflectometry. The observed poloidal wavenumber is chosen by Braggs condition via the tilt angle and the resolution in k-space is determined by the antenna pattern. From the Doppler shift of the reflected wave the poloidal propagation velocity of density perturbations is obtained. The diagnostic capabilities of Doppler reflectometry are investigated using full wave code calculations. The method offers the possibility to observe changes in the poloidal propagation velocity of density perturbations and their radial shear with a temporal resolution of about 10μs.

1. Introduction

Conventional reflectometry (for a review see Laviron *et al* 1996 and Mazzucato 1998) probes the plasma with a microwave signal that travels in parallel to the density gradient in the plasma. From the time delay of the returned signal the radial position of the reflecting layer and thus the background density profile can be obtained. Ideally this wave-plasma interaction can be described as a one-dimensional (1D) problem. 1D density perturbations result in radial movements of the reflecting layer and / or in changes of the index of refraction along the signal path in the plasma. The sensitivity of the measurement on amplitude, shape and radial location of such 1D perturbations has been widely studied both analytically (Mazzucato 1998) and with 1D code calculations (for references see Holzhauer *et al* 1998). For the parameters of present-day fusion experiments it is found that in a 1D geometry the phase response mainly originates from perturbations close to the nominal cut-off layer and their frequency spectrum can be inferred from the spectrum of the measured phase.

The fact that the reflecting surface illuminated by the microwave radiation can have a two-dimensional (2D) structure may seriously perturb density profile as well as density fluctuation measurements. This has been intensively studied both experimentally and by 2D numerical code calculations (for references see Conway 1998 and Holzhauer *et al* 1998). As the wavelengths of density perturbations along the magnetic field lines are much larger than the beam spot size the

structure of the corrugated reflecting layer can be represented by considering the wavevector component perpendicular to the local magnetic field $K_\perp$ only. Thus the reflecting layer is an analogue to a grating in reflection which produces both a 0^{th} order and higher order sidebands in angle space. Depending on amplitude and $K_\perp$-spectrum of the fluctuations the signal measured at the receiver antenna may be no longer coherent and shows strong amplitude fluctuations. Both effects are due to the interference of higher diffraction orders with the reflected 0^{th} order (Holzhauer *et al* 1998).

Asymmetries in the antenna plasma geometry and/or spatially non-symmetric density perturbations result in asymmetric frequency spectra, i. e. in a Doppler shift of the signal reflected from the propagating density perturbations (Bulanin *et al* 1992, Sánchez *et al* 1992, Irby *et al* 1993, Hirsch *et al* 1998, Holzhauer *et al* 1998, Conway 1998, Zou *et al* 1999). A manifestation of such an asymmetry is the phenomenon of the 'runaway phase' which has been observed in almost all reflectometers (for references see Brañas *et al* 1999). A 'runaway phase' occurs in the output of the phase detector due to the interference of (unshifted) 0^{th} order and (frequency shifted) $\pm 1^{st}$ order signal at the receiver antenna (Holzhauer *et al* 1998).

Information about $K_\perp$-spectrum and the propagation velocity of the density perturbations $v_\perp$ can be gained if it is possible to separate the higher diffraction orders from the usually strong 0^{th} order of reflection. For this purpose the line of sight of the antenna arrangement has to be tilted with respect to the normal onto the flux surface, thus preferentially selecting a single diffraction order. Such a Doppler reflectometry experiment is capable to measure the radially resolved propagation velocity of density turbulence $v_\perp(r)$ with a temporal resolution about two orders of magnitude faster than conventional spectroscopic methods. Therefore Doppler reflectometry is well suited to address the topic of velocity shear and shear induced changes of the turbulence spectrum which are thought to be a key element in transitions of anomalous transport (Biglari et al 1990).

In the first part of this paper the principles of Doppler reflectometry are discussed with a simplified model wherein the cut-off layer is replaced by a reflection grid in vacuum illuminated by microwave beam with finite spot size. In Chapter 2 we show experimental results obtained at the W7-AS stellarator with an antenna system where the tilt angle with respect to the reflecting surface was scanned. The diagnostic capabilities and limitations of Doppler reflectometry are discussed in chapter 3 with the aid of 2D full-wave code calculations which take into account the full complexity of the reflection including the effects of refraction and plasma turbulence. Finally we present conclusions resulting from the Doppler reflectometry approach for the further application of reflectometry as a fluctuation diagnostic.

2. Principle of Doppler-Reflectometry

The principle of Doppler reflectometry is shown in Fig.1 where the corrugated cut-off layer is substituted by a reflection grid in vacuum, a treatment that has been designated as 'physical optics model' in (Conway 1998). Conventional reflectometry uses the 0^{th} order of reflection to obtain

information about the distance to the reflecting layer. Radial oscillations of the mirror (e.g. due to long-wavelength MHD modes) lead to a symmetric broadening of the reflected signal frequency spectrum. If the mirror has a small sinusoidal corrugation characterised by a wavenumber $K_\perp = 2\pi/\Lambda_\perp$ the information about $K_\perp$ is contained mainly in the first orders of diffraction which can be selected by the antenna arrangement. As an example in Fig.1 a monostatic antenna is shown with its line of sight tilted by an angle θ_{tilt} with respect to the normal of the reflecting layer. For the -1st order of the diffraction pattern to return to the antenna the Bragg condition requires

$$K_\perp = 2 \cdot k_o \sin(\theta_{tilt}) \tag{1}$$

where k_o is the wavevector of the microwave. Thus by a variation of the tilt angle θ_{tilt} the $K_\perp$-spectrum of the density perturbations can be scanned. We note that for larger corrugation amplitude or non-sinusoidal corrugations higher orders of diffraction have to be taken into account (see chapter 3).

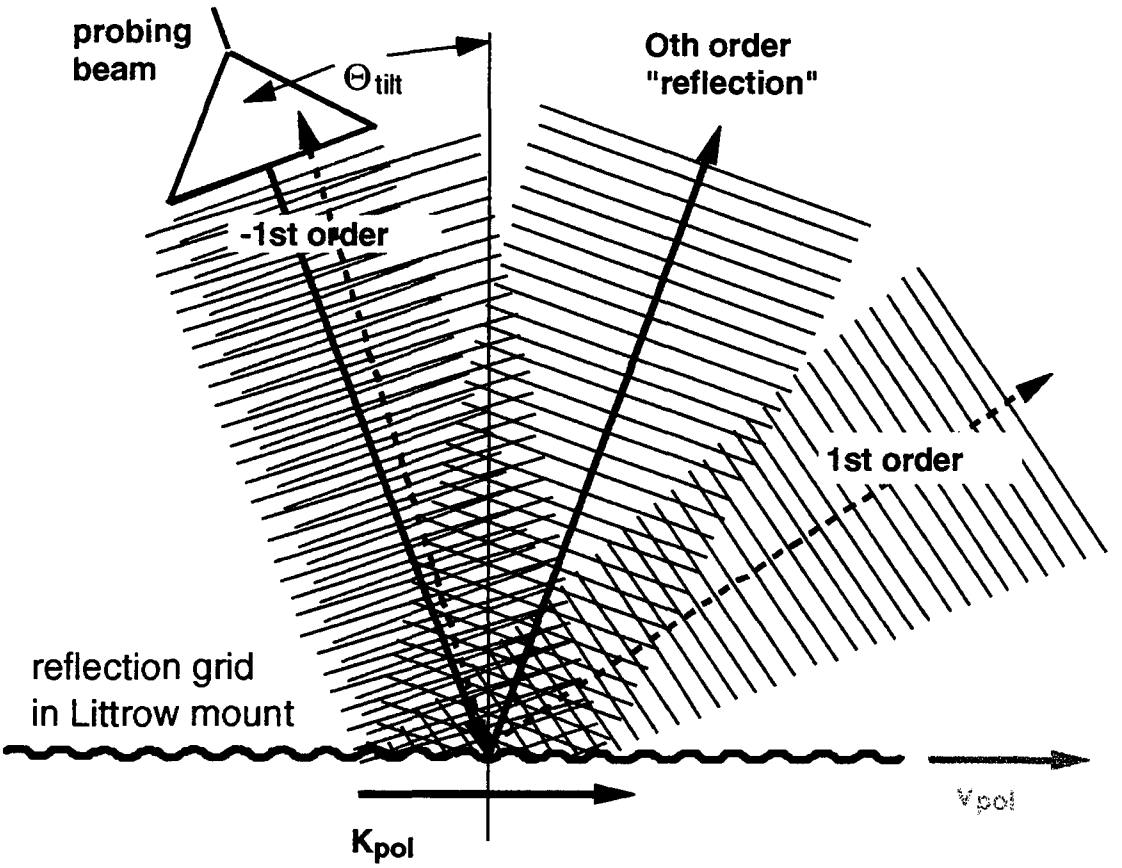

Figure 1. Principle of Doppler reflectometry illustrated using a reflection grid in vacuum and a single antenna arrangement in a Littrow mount.

The resolution of the antenna in $K_\perp$-space is determined by the relation between the width of the illuminated spot and the wavelength of the corrugation. An analytic expression for the $K_\perp$-resolution is possible if the electric field pattern of the antenna has a Gaussian shape $E \propto exp[-x^2/w^2]$ and the reflecting layer is close to the beam waist w. Then the 1/e width of the weighting function for amplitudes in $K_\perp$-space becomes (Holzhauer and Massig 1978)

$$\Delta K_\perp = \sqrt{2} \cdot \frac{2}{w} \tag{2}$$

In Eq.2 it has been assumed that the tilt angle θ_{tilt} is small enough for the effect of the geometric projection of the beam waist onto the reflecting layer $w_{eff} = w/cos(\Theta_{tilt})$ to be neglected. For typical values (beam diameter of a few cm, poloidal wavelengths $\Lambda_\perp \approx 1\,\mathrm{cm}$) the cut-off layer can be considered as a grating where a few poloidal wavelengths are illuminated only. In the limit of large poloidal wavelengths $\Lambda_\perp > 2 \cdot w$ the diffraction orders overlap, i.e. $\Delta K/K > 1$, and the simpler geometrical optics approach is sufficient.

If the reflection grid propagates with a velocity $v_\perp$ the frequency of the wave diffracted in -1st order is shifted by (see Eq. 1)

$$\begin{aligned} \Delta f &= -(2\pi)^{-1} \cdot K_\perp \cdot v_\perp \\ &= -2 \cdot (f/c) \cdot \sin\theta_{tilt} \cdot v_\perp \end{aligned} \tag{3}$$

As a consequence, in a Doppler reflectometry experiment the spectrum in $K_\perp$-space is transferred into a spectrum in frequency space. Higher orders of diffraction, which are selected in $K_\perp$-space by the antenna aperture and the angle θ_{tilt}, are separated from the 0th order of reflection by their finite Doppler shift in frequency space. In the first line of Eq.3 the frequency shift is described as the result of a modulation of the returning microwave by a propagating periodic structure characterised by wavevector $K_\perp$. This description is equivalent to that of a Doppler shift of a wave reflected from a target moving under an angle θ_{tilt} with respect to the normal to the line of sight (second line of Eq.3).

An Doppler shift also may occur due to density perturbations propagating radially with velocity v_r which are equivalent to a partially reflecting mirror. However, the Doppler shift resulting from a radial propagation is $\propto cos\,\theta_{tilt}$ and therefore can be distinguished from a frequency shift according Eq.3 by a variation of θ_{tilt}. Experiments at W7-AS (Brañas *et al* 1999, Holzhauer *et al* 1998) showed that a variation of θ_{tilt} from positive to negative values resulted also in an inversion of the frequency shift. From this it was concluded that for these experiments contributions of the Doppler shift originating from radially propagating density perturbations could be neglected.

Doppler reflectometry may be considered as a hybrid between conventional reflectometry with a reflecting cut-off layer and a standard scattering experiment in a transparent medium : Eqs. 1-3 are equivalent to those of standard scattering from a periodic density perturbation $K_\perp$. The transition to reflectometry is effected by the insertion of a mirror at the position of the nominal cut-off layer. In order to return to the usual scattering formalism the tilt angle θ_{tilt} must be substituted by the deflection angle of the scattering experiment $\vartheta = 2 \cdot \theta_{tilt}$. In the limit of grazing incidence ($\theta_{tilt} = 90^o$) the experiment formally corresponds to backscattering with $\vartheta = 2 \cdot \theta_{tilt} = 180^o$. Doppler reflectometry keeps the K-selectivity of a scattering experiment but overcomes its poor spatial resolution by the use of a cut-off layer in the plasma. Note that a cut-off is also used to obtain spatial resolution also in cross-polarisation scattering experiments (Colas et al 1998).

3. Doppler-Reflectometry Experiments at W7-AS

The geometry of a Doppler reflectometry experiment at the stellarator W7-AS (R= 2.0 m, average minor radius a=0.17 m) is shown in Fig.2. The experiment is performed in a toroidal plane where the poloidal cross section of the stellarator plasma is nearly elliptically shaped and the toroidal magnetic field (B_{tor}(R = 2m) = 2.5 T) increases towards the torus centre similar to a tokamak. The monostatic antenna system is located in the vacuum vessel slightly above the equatorial plane. A corrugated horn in combination with an elliptical mirror result in a Gaussian antenna characteristics $E \propto exp[-x^2/w^2]$ with beam waist $w = 3.3\,cm$ at the reflecting layer, i.e. 52 cm away from the mirror. The mirror can be tilted in poloidal direction by more than 15° corresponding to a vertical movement of the spot at the reflecting surface from +6 cm to -7 cm with respect to the equatorial plane. This geometry has been chosen to minimize the effect of the finite plasma curvature. A variation of the tilt angle allows to find the orientation of the mirror for which the line of sight becomes perpendicular to the flux surfaces which results in a symmetric frequency spectrum. This is necessary as the geometry of the plasma edge of the low-shear stellarator W7-AS can be modified by magnetic island structures with low poloidal modenumber leading to a corrugation of the outer flux surfaces. It turns out that for typical plasma conditions a scan of the mirror tilt leads to a variation of the effective tilt angle between $1^o < \theta_{tilt} < 15^o$.

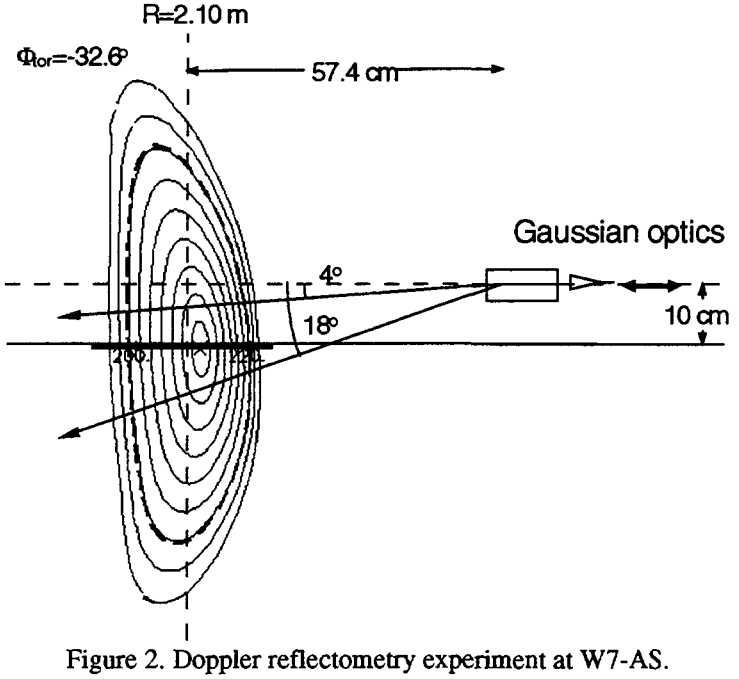

Figure 2. Doppler reflectometry experiment at W7-AS.

Microwave radiation is launched and received in x-mode polarisation with frequencies in the W-band (70-110 GHz) thus probing densities between 1 and 6 10^{19} m^{-3}. The reflecting layer typically lies less than 3 cm inside the plasma boundary as defined by the limiter position or the separatrix. This rather shallow penetration depth is due to the elliptical cross section of the plasma at this toroidal position and the strong edge density gradients observed for most plasmas in W7-AS. Therefore, and also due to the rather short wavelength used ($0.3\,cm < \lambda_o < 0.4\,cm$) refractive effects in the plasma hardly matter and the reflection process can be fairly well approximated by a mirror. This is confirmed by the 2D full-wave code calculations given in chapter 3.

For the experiments either a homodyne reflectometer using a Gunn oscillator as signal source with fixed frequency ($f = 85\,GHz$) or a broadband heterodyne reflectometer system (Hirsch

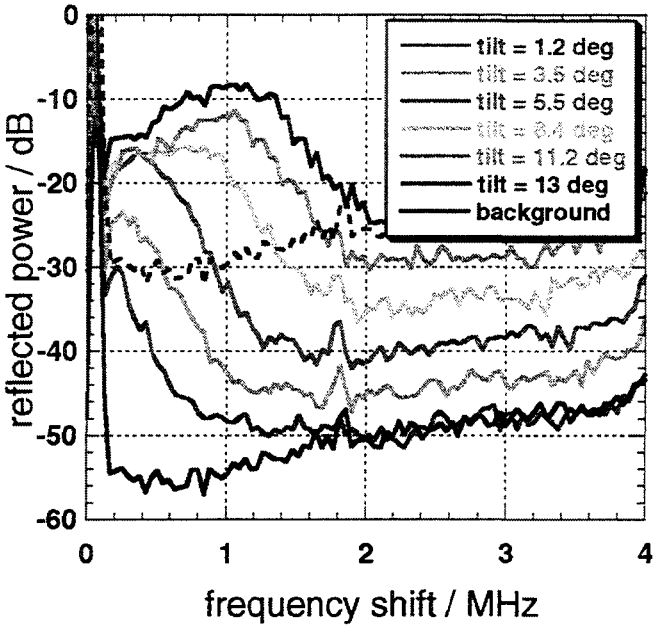

Figure 3. Doppler reflectometry spectra measured with a variation of the tilt angle at fixed effective radial position (r-a)=-1.7 cm of an ECRH heated plasma. The plasma boundary (a=17.3 cm) is defined by the limiter. The spectra are vertically shifted for clarity. Dashed lines indicate the background noise level for the lowest and the uppermost spectrum respectively.

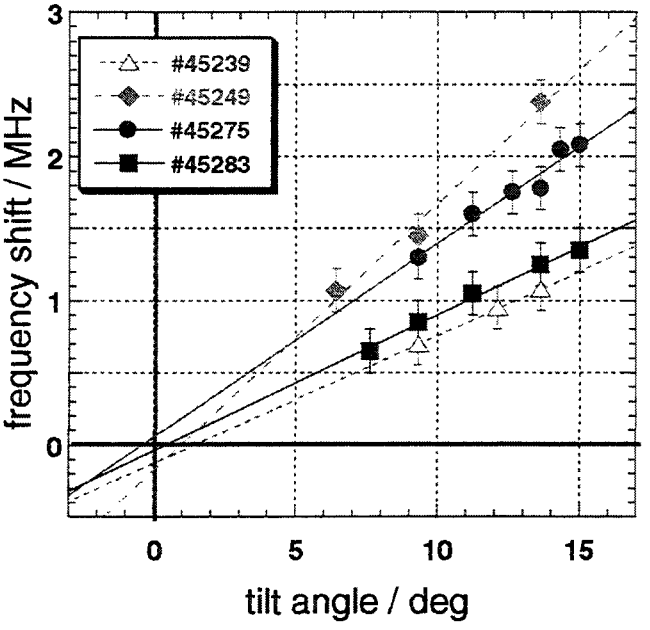

Figure 4. Frequency shift of the spectral feature shown in Fig.3 as a function of θ_{tilt}. As examples four ECRH heated discharges with various magnetic configuration and average density are shown. In any case the probed density is 2 10^{19} m^{-3}.

et al 1996) are used. Final signal procedssing is performed with a spectrum analyser around the last intermediate frequency ($f_{IF} = 60$ MHz) of the heterodyne receiver or around zero-frequency for the homodyne system respectively. A full spectrum is scanned within 20 ms with a resolution $\Delta f = 20$ kHz. In addition up to six bandpass filters with variable centre frequency and bandwidth are available to observe fast changes in the frequency spectrum. Finally a frequency tracker provides an analogue output signal which is proportional to the instantaneous frequency.

For a frequency of 85 GHz (vacuum wavelength of 3.6 mm) the accessible range of poloidal wavevectors is estimated to be $K_\perp < 9\ cm^{-1}$, i.e. accessible poloidal wavelengths are $\Lambda_\perp > 7$ mm. In practice the finite width of the 0th and -1st orders of diffraction determine the minimum frequency shift that can be measured and thus the lower boundary of $K_\perp$ which can be accessed. For a poloidal tilt angle $\theta_{tilt} = 14^o$ a Doppler shift of $\Delta f = 1$ MHz corresponds to a poloidal propagation velocity $v_\perp = 7.4$ km / s. With that velocity the density perturbations pass the probing microwave spot within $\Delta t \approx 9\ \mu s$. It is important to note that $v_\perp$ calculated from the Doppler shift is a local quantity measured at the position of the illuminated spot. In order to obtain the corresponding flux surface averaged velocity v_{pol} the flux compression of the magnetic field topology at the measured position has to be taken into account. Due to the elliptic shape of the poloidal cross section (see Fig.2) the local velocity is increased with respect to the flux surface averaged velocity by about a factor of 2. Equlibrium calculations show that for the chosen position this correction factor changes due to the Shafranov shift from 2 to 3.5 if the central β rises from zero to 1%.

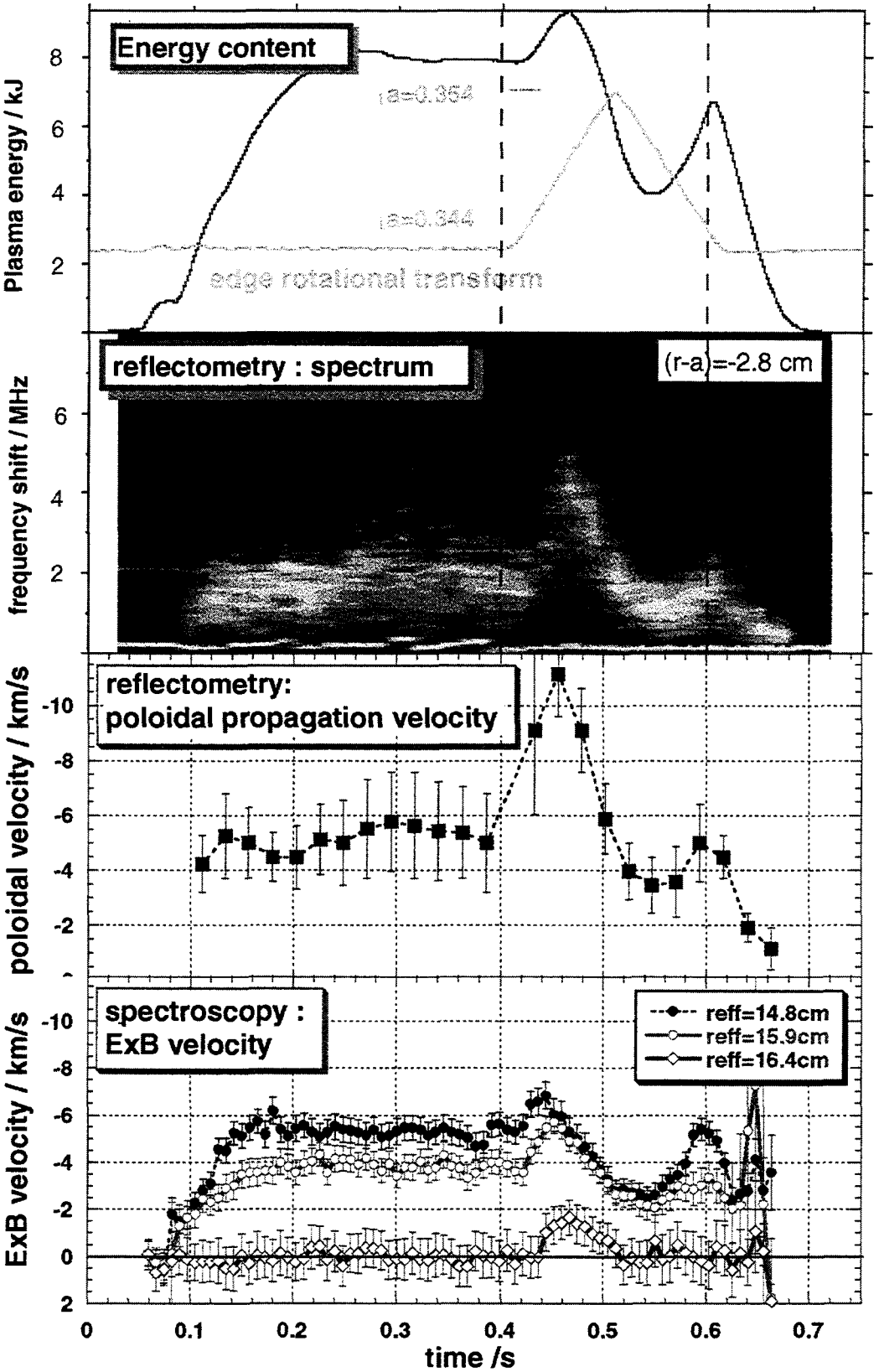

Figure 5. Temporal behaviour measured during a discharge heated with 400 kW ECRH ($< n >= 6.4\ 10^{19}$ m^{-3}). (a) Edge rotational transform ι(a) and diamagnetic energy content. (b) Contour plot of the reflectometry spectrum measured with homodyne detection. (c) poloidal propagation velocity of density perturbations calculated from the Doppler shift in (b). (d) $E \times B$ velocity as measured with passive spectroscopy. The time traces correspond to different radial positions probed with an array of sightlines and show the $E \times B$ velocity shear in the outermost part of the confinement region.

Fig.3 shows a series of spectra obtained with fixed probing frequency while scanning θ_{tilt} on a shot to shot basis using homodyne detection. The reflecting layer is located at an effective radius $(r_{eff} - a) = -1.7$ cm within the plasma boundary as obtained from density profiles measured with beam emission spectroscopy, Thomson scattering and a multichannel interferometer. With increasing θ_{tilt} the peak of the spectrum shifts towards higher frequencies indicating that the antenna selects $K_{pol}(\theta_{tilt})$ from a broad $K_{\perp}$-spectrum. If the tilt angle is too small (typically $\theta_{tilt} < 5^{o}$) the 0^{th} and -1^{st} orders of diffraction cannot be separated in the spectrum. For a number of discharges the frequency shift of this spectral feature is plotted in Fig.4 versus the tilt angle. Within the error bars the observed frequency shift is proportional to the antenna tilt $\theta_{tilt} \approx \sin(\theta_{tilt})$. Thus we conclude that in the accessible range $3\,\mathrm{cm}^{-1} < K_{pol} < 9\,\mathrm{cm}^{-1}$ the poloidal propagation velocity $v_{pol}(K_{pol})$ is almost constant i.e. the dispersion relation of the density perturbations is linear. The value of θ_{tilt} for which the antenna line of sight is perpendicular to the probed cut-off surface can be estimated from a linear extrapolation of the frequency shift down to zero (Fig.4).

An example for the temporal behaviour of the reflected signal in an ECRH heated discharge is given in Fig.5. In the time interval $0.4\,\mathrm{s} < t < 0.6\,\mathrm{s}$ the plasma confinement properties (see Fig.5a) are modified by a small (about 3%) variation of the edge rotational transform $\iota(a)$. During that time reflectometry spectra measured with fixed frequency (Fig.5b) show an transient variation of the Doppler shift. This agrees with the temporal behaviour of the $E \times B$ velocity obtained from the Doppler shift of a BIV emission line (Fig.5d). During the stationary part of the discharge $0.2\,\mathrm{s} < t < 0.4\,\mathrm{s}$ the radial position of the reflecting layer is located at an effective radius $(r - a) = -2.6$ cm inside the plasma boundary defined by the limiter. At the position of the measurement the flux surfaces are compressed by a factor of 2.7 with respect to their average radial distance (see Fig.2). The resulting flux surface averaged poloidal propagation velocity is plotted in Fig.5c. For the steady state time interval $0.2\,\mathrm{s} < t < 0.4\,\mathrm{s}$ one obtains $v_{pol} = 5.5\,\mathrm{km/s}$. Within the error bars this value is identical to the $E \times B$ velocity of the background plasma obtained from spectroscopy for the same radial position (black dots in

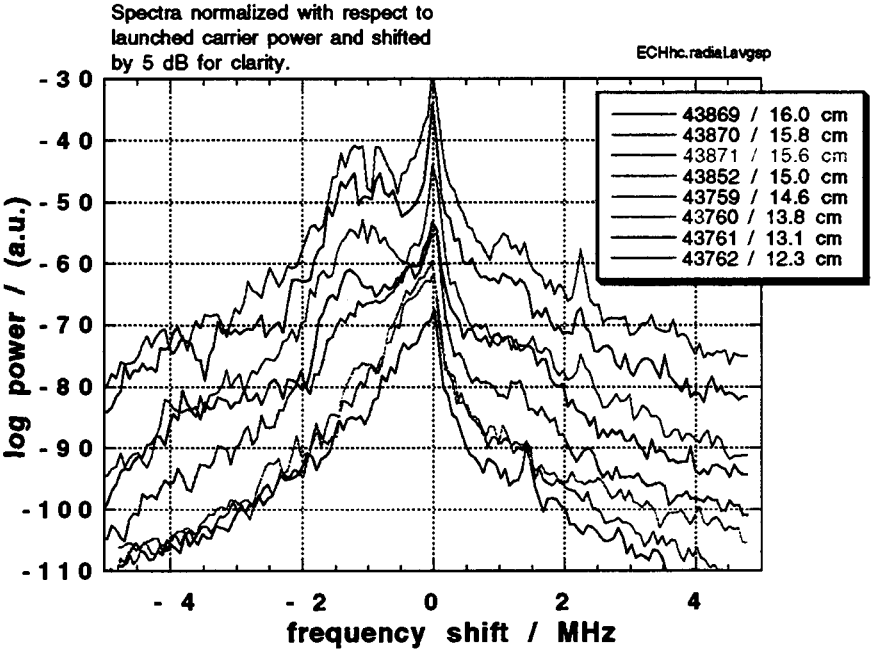

Fig.6: Reflectometry spectra measured with heterodyne detection at different effective radii -1.4cm>(r-a)>-5.1cm in an ECRH heated discharge ($< n > = 7\,10^{19}$ m^{-3}, $\iota(a)$=0.349). The spectra are vertically shifted for clarity.

Fig.5d). Therefore the contribution of the intrinsic phase velocity of the density perturbations on the background plasma to the total poloidal propagation velocity v_{pol} must be small. We note that the incomplete knowledge of the flux compression is the most significant source of error in this comparison of poloidal velocities.

A radial scan of the Doppler reflectometry spectra has been performed using a broadband heterodyne reflectometer (Hirsch *et al* 1996) with its antenna located at an equivalent toroidal position with a similar plasma shape as shown in Fig.2. The *bistatic* Gaussian antenna arrangement has a fixed tilt angle of $\theta_{tilt} = 2.8^{\circ}$. The geometry of a bistatic arrangement is treated in more detail in (Holzhauer *et al* 1998). Due to the tight focussing ($w = 1.9\,\mathrm{cm}$) for a typical frequency of $f \approx 85\,GHz$ the resulting $K_{\perp}$-resolution is $\Delta K/K \approx 1$. Fig.6 shows spectra measured in an ECRH heated discharge at radial positions located between effective radii $-1.4\,\mathrm{cm} < (r_{eff} - a) < -5.1\,\mathrm{cm}$ inside the plasma. The antenna arrangement is oriented in such a way that the red-shifted feature indicates a poloidal propagation of density turbulence in electron diamagnetic direction. Due to the poor $K_{\perp}$-resolution beside the -1st diffraction order also the +1st order enters the receiver antenna, therefore also a weak blue shifted spectral component can be observed with the same frequency shift $|\Delta f|$. The poloidal propagation velocities obtained from the data in Fig.6 are plotted in Fig.7 together with the $E \times B$ velocities derived from active Charge Exchange Recombination Spectroscopy using He as a tracer impurity (Baldzuhn *et al* 1998). In spite of the limited $K_{\perp}$-resolution of this antenna and the ensuing broad spectral features the resolution of the calculated velocity v_{pol} measured with Doppler reflectometry is sufficient to resolve the strong radial shear in the $E \times B$ velocity. Note that this result also provides indirect confirmation of the radial localisation capability of the fluctuation measurement. For the cut-off layer located 5 cm inside the plasma a rather narrow 0th order peak of the reflected signal is seen although the microwave traverses a radial range in which spectra with smaller frequency shift and broadened 0th order of reflection are measured when the cut-off layer is shifted accordingly.

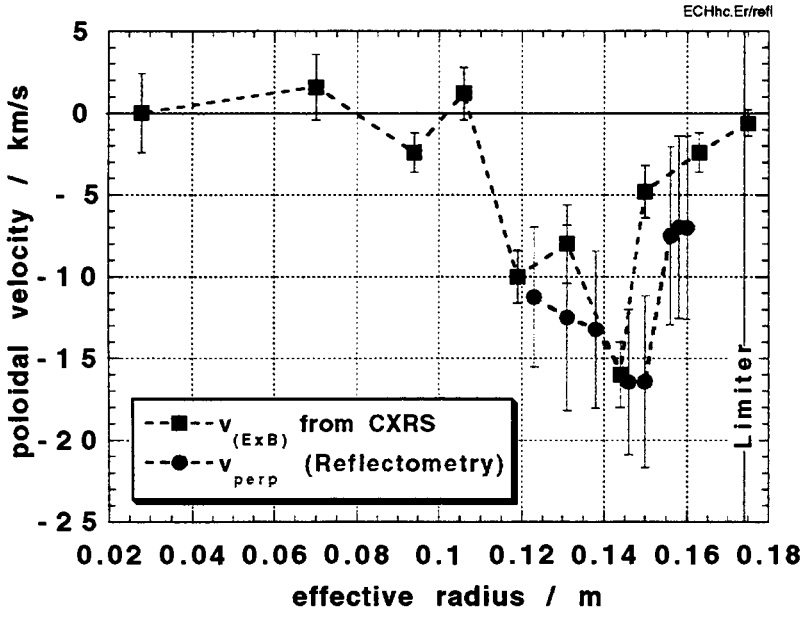

Fig.7: Poloidal propagation velocity of density perturbations obtained from the Doppler shift of the spectral feature in Fig.6 and *ExB* velocity measured with active Charge Exchange Recombination Spectroscopy.

2D full-wave code analysis of Doppler reflectometry

In chapters 2 and 3 Doppler reflectometry experiments were discussed in terms of a moving reflection grating in vacuum. However, in a real plasma the refractive effects due to the background density profile as well as density fluctuations in the transparent region of the plasma affect ingoing and outgoing microwave beams and thus complicate the interpretation of the measurement. These effects are taken into account by 2D full-wave analysis.

4.1. 2D full-wave code analysis

For this study two different full-wave codes have been used :

(1)The RCL-code which uses an equivalent electrical RCL network to represent the propagation of microwaves in a plasma. The implicit calculation yields the stationary solution for the incoming and reflected electric fields at the antenna plane (Holzhauer and Rohrbach 1992, Grossmann *et al* 1997a,b).

(2)The Finite Time Difference (FTD) code, first used by (Irby *et al* 1993). This explicit calculation yields the time dependent solution for the fields over the whole plasma region. As will be demonstrated below the FTD is well suited to visualise the 2D microwave beam pattern and its modification by the plasma.

A third time-independent code has been developed by (Fanack *et al* 1996) which solves the Poisson equation using the implicit biconjugate gradient method. It is planned to undertake a systematic comparison of the numerical codes for which results were presented at this workshop, namely

-> RCL-code as used by E Holzhauer

-> FTD-code as used by B Kurzan and M S Heuraux

-> Poisson equation as used by G Leclert

Note, that for all codes it is only necessary to carry out the time consuming numerical calculations *inside* the plasma region. It is sufficient to define the phase- and amplitude characteristics of the transmitting / receiving beam patterns at the plasma boundary independent of the physical position of the antennas away from the plasma as follows from the reciprocity theorem in inhomogeneous media (Lutomirski and Yura 1971).

4.2. Influence of the stationary background plasma profile:

The refractive effects due to the stationary background plasma are analogous to those in radar experiments in the ionosphere (see e.g. Ginzburg 1964). Their influence on a Doppler reflectometry measurement is as follows :

- Close to the reflecting layer the effective wavelength and effective tilt angle exceed their values in vacuum. Thus the weighting function in $K_\perp$-space and the calculated $v_\perp$ differ from their values estimated for a reflection grid in vacuum
- The Gaussian shape of the beam is distorted. Thus the weighting function for $K_\perp$ changes with respect to the values obtained for vacuum.

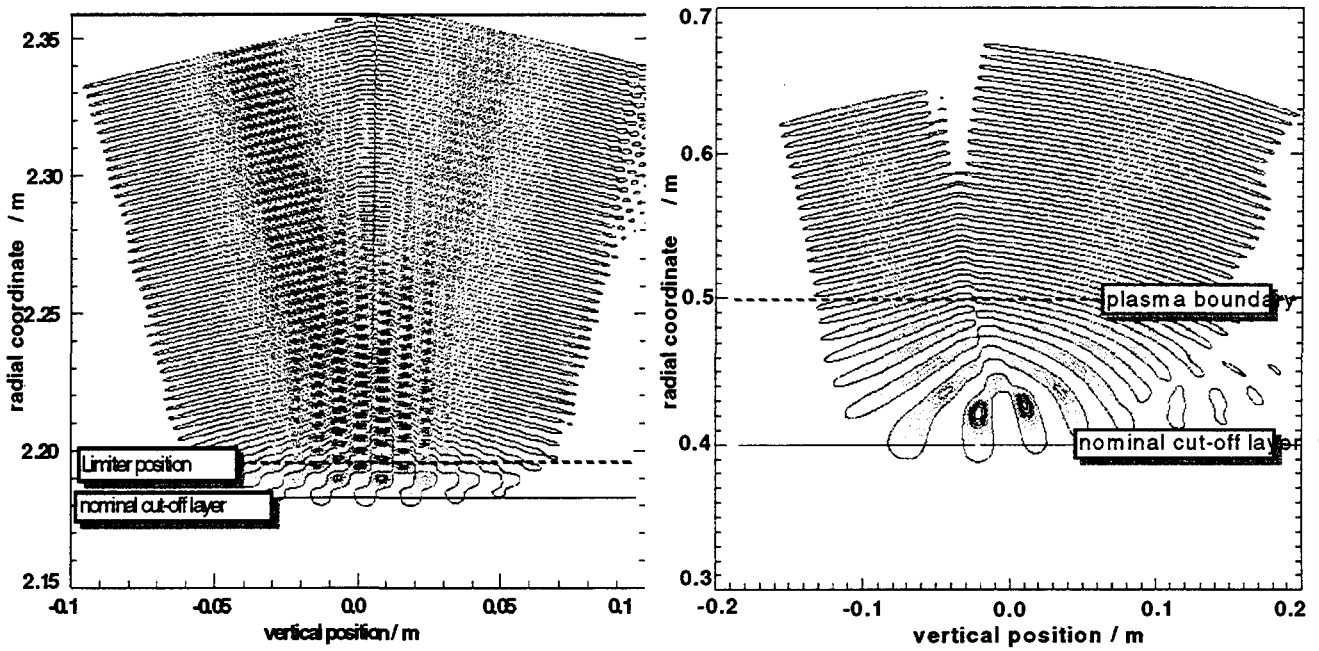

Figure 8. Electric field distributions (Moiré pattern) of the microwave beam calculated with the FTD-code. (a) W7-AS density profile (discharge of Fig.5, t = 300 ms) probed in x-mode polarisation with f=85 GHz. (b) OH discharge of the ASDEX Upgrade tokamak probed with o-mode and microwave frequency f=40 GHz. For both calculations the same antenna characteristics (tilt angle 14°, beam waist w = 3.3 cm) have been used taking into account the background density profile without adding fluctuations.

- With increasing tilt angle the radial position of the cut-off layer shifts radially outward. Depending on the profile shape this shift also may influence the degree of radial localization of the measurement, i.e. the effective width of the probed layer.

Fig.8 shows the calculated electric field pattern of the microwave beam probing two types of plasmas with same antenna tilt angle and Gaussian antenna pattern as used for the measurements in Fig.5 ($\theta_{tilt} = 14^{o}$, beam waist $w = 3.3\,\mathrm{cm}$). In both cases only the background density profile is used without adding density perturbations. As examples we take (Fig.7a) the measured density profile of the W7-AS discharge introduced in Fig.5 probed with microwave frequency $f = 85\,\mathrm{GHz}$ in x-mode polarisation and (Fig.7b) the density profile from an OH discharge of the ASDEX Upgrade tokamak probed with microwave frequency $f = 40\,\mathrm{GHz}$ in o-mode polarisation.

The 2D weighting function for density fluctuations in the plasma can be obtained from the Moiré pattern which is due to the interference of incoming beam and reflected 0^{th} order. It is characterised by the standing wave pattern in the radial and poloidal direction: A cut along the symmetry axis yields the familiar Airy pattern for the standing wave. A cut parallel to the equi-density surface yields the weighting function in the $K_{\perp}$-space. This type of representation is used frequently to illustrate the weighting function in real space in conventional scattering experiments (e.g. Hutchinson 1987). As can be seen in Fig.8a the case of x-mode reflectometry in W7-AS corresponds closely to a 'mirror in vacuum'. In contrast for the o-mode reflectometry at ASDEX Upgrade (Fig.8b) the effective poloidal wavenumber close to the cut-off layer represented by the Moiré pattern is modified. In addition the first radial lobes of the Moiré pattern shift radially

outward if the tilt angle is increased. This is in agreement with the analytical solution (Ginzburg 1968) for the shift of the effective cut-off layer for non-zero tilt angles where as a function of θ_{tilt} the cut-off layer shifts to a position where the index of refraction becomes

$$\mu = \sin(\theta_{tilt}) \tag{4}$$

4.3. Influence of density fluctuations

In the following we consider the case of small amplitude fluctuations where the effects of multiple scattering can be neglected (Born approximation). 2D density fluctuations are represented in the calculations by a change of the local plasma refractive index. This is equivalent to a representation with phase gratings. As an example in Fig.9 the $K_\perp$-sensitivity of the Doppler reflectometry arrangement used for the measurements in Fig.5 is plotted. The continuous line represents the analytic result for a corrugated mirror in vacuum obtained in chapter 2. In order to check the accuracy of the numerical RLC code a thin phase grating is set in vacuum immediately in front of a *plane* mirror and the wavenumber $K_\perp$ of this phase grid is varied. The obtained $K_\perp$-spectrum (open circles in Fig.9) is in excellent agreement with the analytic result.

With increasing fluctuation amplitude the Born approximation is no longer valid and multiple scattering must be taken into account. In addition an increasing amount of the microwave power is diffracted into higher orders even for a sinusoidal phase grating. A full discussion of these effects is beyond the scope of this contribution. An example of numerical calculations performed for strong turbulence-like fluctuations produced by an Edge Localised Mode and the comparison with the reflectometry experiment at W7-AS can be found in (Holzhauer *et al* 1998).

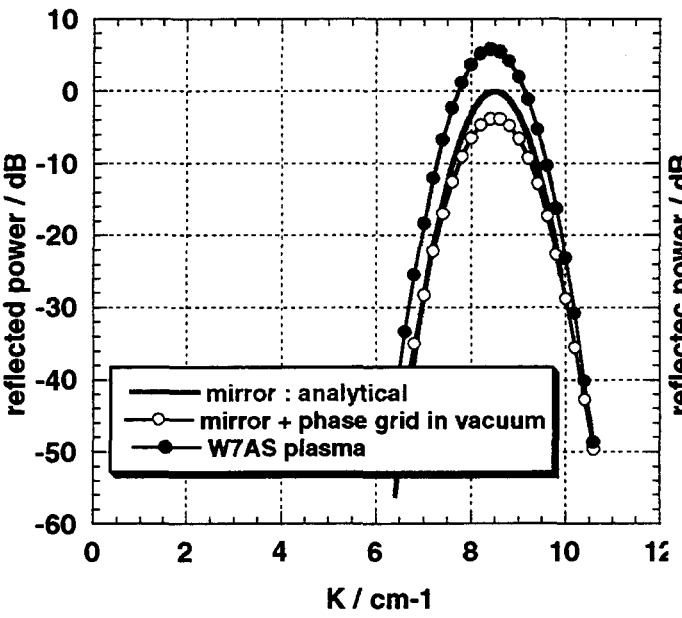

Fig.9 *K*-sensitivity of the antenna calculated with the parameters for the discharge used in Fig.5 (tilt angle 14°, beam waist w = 3.3 cm). Continuous line: analytic calculation (see chapter 2), open circles: plane mirror with phase grating in vacuum, filled circles: density profile of W7-AS discharge with phase grating at the radial position of the last lobe of the Airy pattern.

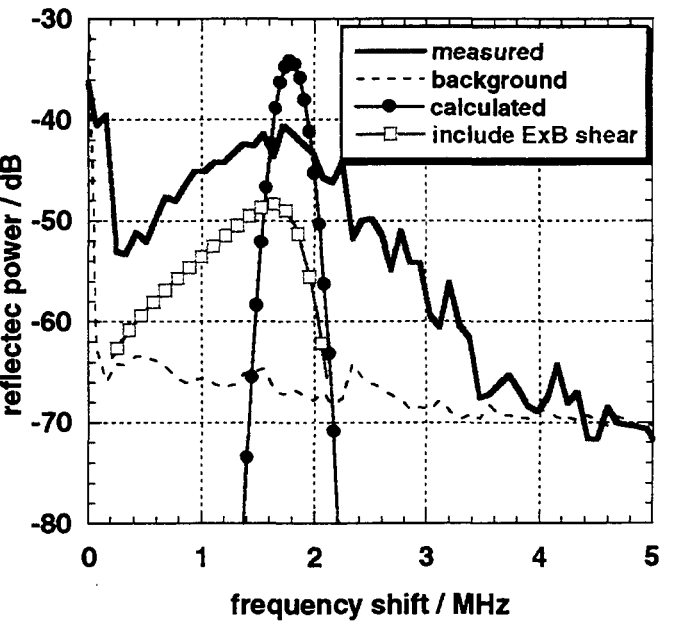

Fig.10 Measured (continuous line) and calculated (filled circles) frequency spectra for the example discharge (see Fig.5). The calculated spectrum is asymmetrically broadened if the *ExB*-velocity shear is taken into account (open squares).

4.4. Comparison of measured and calculated Doppler reflectometry spectra

In Fig.9 the resolution in $K_\perp$-space is calculated with the measured W7-AS density profile for the discharge in Figs.5 and 8a. The wavenumber of a thin phase grating positioned within the last lobe of the Airy pattern is varied. Neither the centre nor the width of the weighting function differ markedly from the vacuum solution. Apparently for the steep density profiles in W7-AS the narrow region with plasma in front of the cut-off layer does not have a significant influence on the microwave propagation as compared with the vacuum case.

In Fig.10 the calculated $K_\perp$-spectrum is transformed into a frequency spectrum $f = (2\pi)^{-1} \cdot K_\perp \cdot v_\perp$ by scaling with a value of $v_\perp$ for which the maxima of calculated and measured spectra fit. The measured frequency spectrum is markedly broader than expected from the RCL code calculations. Several possible mechanisms can contribute to this broadening:

- A finite lifetime of the fluctuations. The width of the spectral feature in Fig.10 would require a lifetime of $\approx 2\ \mu s$.
- An additional broadening of the spectral feature originates from the $E \times B$-velocity shear. This broadening has been taken into account in the calculations (broken line in Fig.9) using the $E \times B$-velocity shear as measured for this discharge with passive spectroscopy. The nominal cut-off is ≈ 1 cm inside the plasma (laboratory coordinates, see Fig7a) and close to the maximum value of the radial electric field $|E_r(r)|$. Therefore the reflectometer is also sensitive to a radial region with lower $E \times B$-velocity resulting in an asymmetric spectral broadening towards lower frequencies.
- A non-stationary behaviour of fluctuations results in a broadening of the spectra which, like in Fig.10, are measured during a time window of 20 ms. In this example - like in many W7-AS discharges - the plasma edge fluctuations show a burst-like behaviour similar to small ELMs rather than a stationary fluctuation level (Hirsch et al 1998a,b). Time resolved measurements with a temporal resolution of $\approx 10\ \mu s$ using bandpass filters show that during these ELM-like events the signal power increases especially at the high frequency side of the spectral feature.

5. Summary and Outlook

Doppler reflectometry is an extension from conventional reflectometry, which ideally measures a 1D (radial) position and movement of the reflecting layer, to a scattering-like diagnostic sensitive to 2D (poloidal) density perturbations. In most operational reflectometers contributions from radial and poloidal perturbations overlap. For many plasma conditions this results in serious complications for the interpretation of the measurements. Here we outline possible consequences arising from the Doppler reflectometry approach for both types of measurements :

For conventional reflectometry the perturbation by the two dimensionality of the reflecting layer can be reduced if one uses the $K_\perp$-selectivity of the antenna in order to separate the

perturbing higher orders of diffraction from the 0th order of reflection which carries the radial information. Consequently at zero tilt angle a broad antenna pattern with a high $K_\perp$-resolution and directivity - the latter can be achieved at the waist of a Gaussian beam - is required. Such a reflectometer has a reduced sensitivity to turbulence with small poloidal scalelength with benefits for the background density profile measurement. Furtheron such a diagnostic can be used for the detection of large scale density perturbations e.g. MHD activity.

As a diagnostic for small scale poloidal density perturbations Doppler reflectometry keeps the K-selectivity of a scattering experiment but by the use of a cut-off layer it overcomes the poor spatial resolution of scattering from comparable K. Thus Doppler reflectometry allows access to two *local* quantities, namely poloidal propagation velocity and K-spectrum of turbulence which are closely connected in the question of shear decorrelation. Time resolved measurements of the shear in v_{pol} can be realised with a two-frequency Doppler reflectometer system. An imaging receiver instead of a monostatic antenna arrangement would allow simultaneous access to 0^{th} and higher diffraction orders of the full K-spectrum. If the phase relations between the received signals are taken into account the diagnostic has the potential for a time dependent (holographic) reconstruction of the density perturbations. Such a system ultimately combines the concept of conventional reflectometry with the sensitivity to poloidal density perturbations.

References

Baldzuhn J, Kick M, Maassberg H and the W7-AS Team 1998 *Plasma Phys. Control Fusion* **40** 967

Biglari H, Diamond P H, Terry P W 1990 *Phys. Fluids B* **2**(1) p 1

Brañas B, Hirsch M, Sánchez J, Zhuravlev V 1999 *Rev. Sci. Instrum* **70**(1) 1025

Bulanin V V and Korneev D O 1992 *Proceedings of the 1st IAEA Tech. Comm. Meeting on Microwave Reflectometry for Fusion Plasma Diagnostics* p184

Colas L et al 1998 *Nuclear Fusion* **38**(6) 903

Conway G D, Schott L, Hirose A 1996 *Rev. Sci. Instrum.* **67** 3861

Conway G D 1998 *Plasma Phys. Control Fusion* **41** 65

Fanack C et al 1996 *Plasma Phys. Control. Fusion* **38** 1915

Grossmann M T, Holzhauer E, Hirsch M, Serra F, Manso M E, Nunes I 1997a *Proc. 24th EPS Conf. on Controlled Fusion and Plasma Physics (Berchtesgaden, 1997)* (Geneva: EPS) IV-1497

1997b *Proceedings of the 3rd Workshop on Microwave Reflectometry for Fusion Plasma Diagnostics (Madrid 1997)* (Informes Tecnicos, CIEMAT, Madrid)

Ginzburg V L 1964 *The Propagation of Electromagnetic Waves in Plasmas* (Pergamon, Oxford)

Hirsch M, Hartfuss H J, Geist T, De La Luna E 1996 *Rev. Sci. Instrum.* **67** 1807

Hirsch M et al 1998a *Plasma Phys. Control. Fusion* **40** 631

Hirsch M et al 1998b *Proc. 25th EPS Conf. on Controlled Fusion and Plasma Physics (Praha,*

1998) (Geneva: EPS) 2322

Holzhauer E and Massig J H 1978 *Plasma Phys. Control. Fusion* **20** 867

Holzhauer E and Rohrbach G 1992 *Proceedings of the 1st IAEA Tech. Comm. Meeting on Microwave Reflectometry for Fusion Plasma Diagnostics (Abingdon 1992)* p89

Holzhauer E, Hirsch M, Grossmann T, Brañas B, Serra F 1998 *Plasma Phys. Control. Fusion* **40** 1869

Hutchinson I H 1987, *Principles of Plasmadiagnostics* , Cambridge, University Press

Irby J, Horne S, Hutchinson I, Steek P 1993 *Plasma Phys. Control Fusion* **35** 601

Laviron C, Donné A J H, Manso M E and Sanchez J 1996 *Plasma Phys. Control. Fusion* **35** 905

Lutomirski R F and Yura H T 1971 *Appl. Optics* **10** 1652

Mazzucato E 1998 *Rev. Sci. Instrum.* **69(6)** 2201

Mazzuccato E 1998b *Rev. Sci. Instrum.* **69(4)** 1691

Sánchez J, Estrada T, Hartfuss H J 1992 *Proceedings of the 1st IAEA Tech. Comm. Meeting on Microwave Reflectometry for Fusion Plasma Diagnostics (Abingdon 1992)* p133

Vershkov V A, Dreval V V, Soldatov S V, Traun S V, Kartsev Y A 1995 *Proc. 22nd EPS Conf. on Controlled Fusion and Plasma Physics (Bournemouth, 1995)* vol. IV (Geneva: EPS) p 401

Zou X L et al 1999 this workshop